Journal of Catalysis 337 (2016) 102–110

Contents lists available at ScienceDirect

Journal of Catalysis

journal homepage: www.elsevier.com/locate/jcat

Adsorbed species on Pd catalyst during nitrite hydrogenation approaching complete conversion

Yingnan Zhao [a], Nidadavolu Koteswara Rao [a], Leon Lefferts [a,b,*]

[a] Catalytic Processes and Materials, MESA+ Institute for Nanotechnology, University of Twente, Enschede 7500AE, The Netherlands
[b] Aalto University, School of Chemical Technology, Department of Biotechnology and Chemical Technology, P.O. Box 16100, 00076 Aalto, Finland

ARTICLE INFO

Article history:
Received 22 April 2015
Revised 11 January 2016
Accepted 3 February 2016

Keywords:
Pd
Nitrite hydrogenation
Selectivity
Mechanism
ATR-IR

ABSTRACT

Pd catalysts are well known for their ability to hydrogenate nitrite to form molecular nitrogen as well as ammonium. Removal of nitrite and nitrate form drinking water requires extreme high selectivity to molecular nitrogen. This work shows that selectivity to ammonium can suddenly rise when complete conversion of nitrite is achieved in semi-batch operation. Surprisingly, formation of ammonium is continuing after exhaustion of nitrite. These observations were confirmed for unsupported colloidal Pd particles stabilized with PVA, colloid Pd NPs supported on Al_2O_3, as well as conventional Pd/alumina catalysts prepared via impregnation. The amount of ammonium formed after exhaustion of nitrite was quite similar to the number of accessible Pd surface sites, indicating that N-containing species adsorbed on the Pd surface are responsible for the effect. ATR-IR experiments prove that the responsible adsorbed species is not IR active and we propose that the surface of the catalyst is importantly covered with rather unreactive atomic nitrogen. These N atoms are almost unreactive, and neither the formation of ammonium via hydrogenation, nor the formation of N_2 via dimerization contribute significantly during steady-state operation.

1. Introduction

Nitrate and nitrite are harmful compounds often found in underground drinking water supplies, especially in agricultural areas using nitrogen-rich fertilizers. In the late 1980s, the pioneering work by Vorlop and co-works has shown that nitrate can be reduced to nitrogen (N_2) using bimetallic hydrogenation catalysts, with nitrite as intermediate and ammonium as by-product, via reaction shown in Eqs. (1)–(3) [1–3]. Since then, various metals have been tested in order to optimize activity and selectivity to N_2, minimizing the formation of ammonium [4–12].

$$NO_3^- + H_2 \xrightarrow{Pd-Cu} NO_2^- + H_2O \quad (1)$$

$$2NO_2^- + 3H_2 + 2H^+ \xrightarrow{Pd} N_2 + 4H_2O \quad (2)$$

$$NO_2^- + 3H_2 + 2H^+ \xrightarrow{Pd} NH_4^+ + 2H_2O \quad (3)$$

Palladium has been found as most active catalyst for nitrite hydrogenation (Eqs. (2) and (3)), with the best selectivity to N_2 [2,7]. Studies have been extensively performed in order to understand the mechanism of the reaction with Pd catalysts. It has been well accepted that the turn-over-frequency (TOF) of the reaction is independent of the Pd particle size [13–15]. Yoshinaga et al. first claimed a relationship between the structure of Pd nanoparticles (NPs) and the selectivity, using supported Pd catalysts in fixed bed operation [16]. Our previous work with unsupported Pd colloids showed that a large Pd particle size is favorable for the formation of ammonium in semi-batch reaction with continuous hydrogen flow [15].

The objective of this study was to gain better insight into the mechanism of nitrite hydrogenation on Pd NPs supported on Al_2O_3 in order to understand the product distribution, i.e. high selectivity for formation of molecular nitrogen. The catalysts are prepared with colloidal methods as well as impregnation methods. We will show that selectivity changes dramatically when approaching full conversion; the consequences for the mechanism of the reaction will be discussed.

* Corresponding author at: Catalytic Processes and Materials, MESA+ Institute for Nanotechnology, University of Twente, Enschede 7500AE, The Netherlands. Fax: +31 53 489 4683.
E-mail address: l.lefferts@utwente.nl (L. Lefferts).

http://dx.doi.org/10.1016/j.jcat.2016.02.007
0021-9517/

2. Experimental

2.1. Chemicals

Sodium tetrachloropalladate (II) ($Na_2PdCl_4 \geqslant 99.995\%$), polyvinyl alcohol (PVA, average MW = 13,000–23,000, 87–89% hydrolyzed), and sodium borohydride ($NaBH_4$, $\geqslant 96\%$ (gas-volumetric) were purchased from Sigma–Aldrich. Palladium acetylacetonate ($Pd(acac)_2 \geqslant 99\%$) was purchased from Alfa Aesar, and acetone (>99%) and 2-propanol (>99%) were purchased from Merck. γ-Al_2O_3 (S_{BET} = 205 $m^2\ g^{-1}$) was supplied by BASF. Sodium nitrite (>99%) was purchased from Merck. All the aqueous solutions were prepared using ultra purified water obtained on water purification system (Millipore, Synergy).

2.2. Pd-PVA colloid

The preparation of palladium nanoparticles via colloidal method has been described in our previous paper, which can be summarized as follows [17]. PVA was dissolved in water at 70 °C with stirring for at least 2 h. The solution (2 wt%) was then cooled down to room temperature. Aqueous solution of Na_2PdCl_4 (20 mL, containing 0.086 mmol Pd) and 1.76 mL of freshly prepared PVA solution were added to 240 mL water, obtaining a yellow–brown solution. After 3 min, $NaBH_4$ solution (1.72 mL, 0.172 mmol) was added under vigorous stirring. The brown Pd colloid solution was immediately formed. The final pH was typically 8–8.5.

2.3. Pd-PVA/Al_2O_3

γ-Al_2O_3 (38–42 μm) was calcined in airflow at 600 °C for 4 h before adding 1.5 g γ-Al_2O_3 to 520 mL as-prepared Pd-PVA colloidal suspension (Pd-concentration 3.3×10^{-4} mol L^{-1}) without any pH adjustment. After stirring with a mechanical 6-blade-stirrer (∅44 mm, 1000 rpm) with the propeller positioned at the center of liquid for 2 h, the catalyst was filtered and dried in a vacuum oven at 40 °C

2.4. Pd/Al_2O_3

Pd nanoparticles supported on the same calcined γ-Al_2O_3 were also prepared via wet impregnation method in order to compare with Pd-PVA/Al_2O_3. Typically, 0.95 g of γ-Al_2O_3 was added into 80 mL acetone solution containing 4.7×10^{-4} mol L^{-1} $Pd(acac)_2$. Then the suspension was stirred with a magnetic stirrer (500 rpm) for 3 h, followed by drying using a rota evaporator (IKA Labortechnik) under sub-atmospheric pressure at 80 °C. The resulting sample was calcined at 300 °C in airflow for 3 h, and subsequently reduced in H_2 at the same temperature for 3 h.

The prepared catalysts were stored in air. No further pretreatment was performed before any experiments described below unless specified otherwise.

2.5. Characterization

Pd particle size distribution was determined using TEM (CM300ST-FEG, Philips) with a resolution of 1 nm. The Al_2O_3 supported catalysts were firstly ground into sub-micron fragments and dispersed in ethanol. Then the suspension was dropped on a copper grid covered with hollow carbon for taking TEM images. At least five of these ground fragments were randomly selected for determination of Pd particle sizes, and typically 300 Pd particles were measured. Note that information on the spatial distribution of nanoparticles through the support cannot be obtained as the samples were ground. The metal loading on the supports was analyzed by XRF (PW 1480, Philips). The total surface area of samples was calculated based on N_2 physisorption (ASAP 2400, Micromeritics) data, using the BET theory with a typical error margin of 5%.

The zeta potential of the catalysts dispersed in aqueous phase was measured with a Zetasizer Nano ZS ZEN3600 instrument (Malvern Instruments) at 25 °C using a laser with wavelength of 633 nm. The pH was adjusted to 6 with HCl and NaOH solution.

CO chemisorption at room temperature was used to determine the metal surface area that is accessible in gas phase (Chemisorb 2750, Micromeritics). Typically, the sample was pre-reduced at room temperature in hydrogen and then flushed in He at the same temperature. Then CO was introduced as pulses and the responses were recorded using a TCD detector. We assumed that the stoichiometric ratio of number of adsorbed CO molecules and number of accessible Pd surface atoms is 1:1. The Pd dispersion (*Pd disp.*) was defined as

$$Pd\ disp. = \frac{\text{number of Pd atoms in the surface of NPs}}{\text{number of Pd atoms in total}}$$

2.6. Nitrite and ammonium adsorption in aqueous phase

Adsorption isotherms for nitrite and ammonium were determined using a home-built apparatus containing a flat bottom flask (250 mL) with a magnetic stirrer at room temperature. Typically 50 mg catalyst was added to 100 mL H_2O and stirred, dispersing 10% CO_2/Ar (1 bar, 40 mL min^{-1}) in the suspension for at least 1 h. Then 1 mL of concentrated sodium-nitrite or ammonium-chloride solution was injected into the suspension, repetitively every 15 min. Adsorption equilibrium was achieved within 5 min and one sample of 1 mL was taken when equilibrium was achieved after each injection, using a syringe equipped with a filter (PTFE, 0.2 μm) to remove the catalysts. The samples were analyzed for nitrite or ammonium with ion chromatography (IC, ICS 1000, DIONEX). The amount of nitrite or ammonium adsorbed was calculated by subtracting the amount of nitrite or ammonium in solution, calculated based on the equilibrium concentration, from the total amount of nitrite or ammonium added.

2.7. ATR-IR of nitrite hydrogenation

A suspension containing 0.1 g Pd/Al_2O_3 dispersed in 25 mL 2-propanol was spray coated on a trapezoidal ZnSe crystal (52.5 mm × 20 mm × 2 mm, facet angle 45°, Anadis instruments BV), resulting in about 5 mg catalyst on the crystal, which was then mounted in a home-build *in-situ* Attenuated Total Reflection Infrared Spectroscopy (ATR-IR) cell which has been described in detail elsewhere [18]. The chamber above the ATR crystal in the cell was about 0.77 mL in volume. The cell was mounted in the sample compartment of an infrared spectrometer (Tensor 27, Bruker) equipped with a MCT detector. All the measurements were done at room temperature (21 ± 1 °C) with a resolution of 4 cm^{-1}. Nitrite hydrogenation on the catalyst was performed via a multi-step titration method:

(1) Typically the catalyst was first flushed with water saturated with hydrogen (flow rate = 1 mL min^{-1}, p_{H2} = 1 bar) for 4 h in order to remove adsorbed oxygen from Pd surface.
(2) Followed by flowing water saturated with argon for 30 min, in order to remove any physisorbed hydrogen on the catalyst as well as residual hydrogen in liquid phase.
(3) After that, nitrite solution (0.025 mol L^{-1}, argon saturated, 1 mL min^{-1}) flow was introduced into the cell during 30 min in order to adsorb nitrite on the catalyst.
(4) Argon saturated water was then used again for 10 min to remove residual nitrite in solution as well as any physisorbed nitrite on the catalyst.

(5) Finally, water saturated with hydrogen was introduced, reacting with nitrogen-containing-species (*N*-species) adsorbed on the catalyst, until the IR signals from nitrogen containing species either adsorbed on the catalyst or present in the liquid became constant.

All the liquid flows were pumped by a peristaltic pump (Masterflex) downstream of the ATR-IR cell and then directed to a container.

After completion of the five steps described above, a recirculation flow study was performed in order to mimic a semi-batch reaction at almost-complete-conversion level. The H_2/H_2O flow was stopped, while the flow exiting the ATR-IR cell was directed back to the entrance of the ATR-IR cell, passing through a porous alumina tube (inner diameter 1.0 mm, outer diameter 1.8 mm, length 65 mm), coated with polydimethylsiloxane (PDMS) membrane. The function of the semi-permeable membrane tube is to introduce additional H_2 to the recirculating liquid, by allowing H_2 molecules to diffuse through the PDMS membrane from H_2 gas flow at the outside of the tube. The amount of liquid in the cell, the tubes and the pump is about 2.5 ml. The recirculation flow was maintained during 150 min, and ATR-IR spectra were taken using the same resolution and speed as described above.

2.8. Nitrite hydrogenation

The reaction was performed in a home-build semi-batch reactor including a glass tank reactor (∅98 mm with four 5 mm baffles), equipped with a mechanical 6-blade-stirrer (∅44 mm, 1000 rpm) with the propeller positioned at the center of liquid. Typically, 50 mg catalyst was dispersed in 300 mL H_2O. The mixed suspension was then stirred vigorously in $H_2/He/CO_2$ atmosphere to reduce the catalyst ($H_2/He/CO_2$ = 6/3/1, total flow rate = 100 mL min^{-1}, total pressure = 1 bar) for at least 1 h. CO_2 was used as a buffer to control pH to 5.5 ± 0.5.

The reaction was initiated by injecting 3 mL $NaNO_2$ solution (44 mmol L^{-1}). Samples of the reaction suspension of 1 mL were taken with syringes equipped with filters (PTFE, 0.2 μm) to remove the catalyst. Samples were taken every 5 min and then injected into the IC (DIONEX, ICS 1000) to determine the concentration of nitrite and ammonium. The rate of formation of N_2 is calculated as the difference between the rates of nitrite conversion and ammonium formation.

Experiments in a continuous operated fixed bed reactor were performed to check for any catalysts deactivation for Pd-PVA/Al_2O_3 and Pd/Al_2O_3. The equipment used is described in detail in the Supporting Information.

In addition, nitrite hydrogenation with semi-batch operation with Pd-PVA is performed, followed by adding concentrated $NaNO_2$ solution (3 mL, 44 mmol L^{-1}) after achieving 95% nitrite conversion in the first run. Samples are also taken every 5 min and analyzed in IC as described above.

3. Results

3.1. TEM

Fig. 1 shows typical TEM images of unsupported Pd-PVA and Pd-PVA supported on Al_2O_3. Unsupported Pd-PVA showed sphere-like shaped particles with an average size of 2.2 nm (Table 1), whereas Pd NPs deposited on Al_2O_3 seem somewhat distorted, suggesting hemi-spherical shaped particles with an apparent particle size of 3.0 nm. The changes of Pd particle size and shape indicate that the PVA stabilized particles interact significantly with alumina.

3.2. Zeta potential

As shown in Table 1, the zeta potential of unsupported Pd-PVA colloid was negative at pH = 6, whereas the colloid supported on Al_2O_3 was positively charged at the same pH.

3.3. Adsorption

3.3.1. Nitrite adsorption

Fig. 2(a) shows that equilibrium of nitrite adsorption on Al_2O_3 was reached rapidly within 1 min; the initial concentration was 275 μmol L^{-1}, rapidly decreasing to the equilibrium concentration (175 μmol L^{-1}). Similar fast equilibrium was observed with Pd-PVA.

The coverage of alumina surface by NO_2^- ($\Gamma_{NO_2^-}$) can be estimated with the following equation:

$$\Gamma_{NO_2^-} = \frac{M_{NO_2^-,surface}}{(S_{surface}/S_{NO_2^-})/(6\times 10^{23})} \times 100\% \quad (4)$$

where $M_{NO_2^-,surface}$ is the amount of nitrite adsorbed on Al_2O_3 in moles, which can be estimated based on the data in Fig. 2(b). $S_{surface}$ is the specific area as determined by N_2 physisorption with the BET method (Table 1). $S_{NO_2^-}$ is the area occupied by a NO_2^- ion, estimated at 4×10^{-20} m^2, assuming the size of NO_2^- ion is 0.2 nm. Fig. 2(b) shows that the maximal coverage achieved in Fig. 2(b) is as low as 0.02%. Note that the detection limitation of the IC is 0.5 μmol L^{-1} and that equilibrium concentration is achieved when about 8×10^{-4} μmol m^{-2} nitrite is adsorbed. The resulting surface-coverage of NO_2^- ions on alumina is as low as 0.002%, illustrating the sensitivity of this technique.

In contrast, nitrite adsorption on Pd-PVA (Fig. 2(c)) results in a much higher coverage, assuming that CO chemisorption in aqueous phase is a good measure for the number of Pd surface atoms available for interaction with nitrite [15]. For example, 8% of the Pd surface sites accessible, as described above, is covered with NO_2^- when in equilibrium with 0.5 μmol L^{-1}. The estimated coverage can be as high as 240% in equilibrium with nitrite concentration equal to 80 μmol L^{-1}. Probably, nitrite adsorption on PVA contributes significantly to explain this high value. Note that the samples were used without pre-reduction with H_2, and therefore it cannot be ruled out that oxygen chemisorbed on the Pd surface reacts with nitrite, contributing to disappearance of nitrite. However, IC detected no NO_3^- in the solution in all experiments. In any case, the surface coverage of NO_2^- on Pd is clearly significant.

3.3.2. Ammonium adsorption

Fig. 3(a) shows that ammonium adsorption on Al_2O_3 also equilibrated rapidly within a few minutes. Fig. 3(b) shows the adsorption isotherm of ammonium on Al_2O_3. The result in terms of surface coverage is similar to the results with nitrite, revealing very weak interaction of alumina with both nitrite and ammonium, and very low coverages.

3.4. ATR-IR

Fig. 4(a)–(c) shows typical spectra of nitrogen-containing species adsorbed on Pd/Al_2O_3 catalyst during exposure of a hydrogen covered Pd catalyst to nitrite. The species identified in the IR spectra include linear- and multi-bonded NO (NO (L) and NO (M)) on Pd at 1710 cm^{-1} and 1580 cm^{-1}, respectively, as well as a NH_2 intermediate at 1490 cm^{-1}. The peak at 1450 cm^{-1} is assigned to NH_4^+, produced exclusively initially. The peak at 1235 cm^{-1} represents free nitrite ions in aqueous phase. These assignments have been discussed in detail in previous work [19,20].

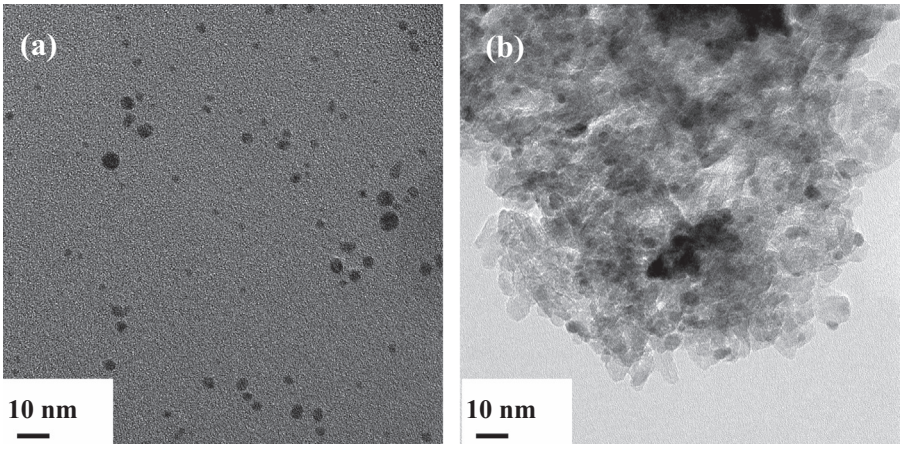

Fig. 1. TEM images: (a) Pd-PVA colloid; (b) 2.7 wt% Pd-PVA/Al_2O_3.

Table 1
Physical properties of samples in this study.

Sample	Pd loading (wt%)	$D_{Pd,TEM}$ (nm)	S_{BET} ($m^2\ g^{-1}$)	Pd disp. (%)	$\zeta_{pH=6}$ (mV)
Pd-PVA		2.2 ± 0.7		9[a]	−34.5
Al_2O_3			205		26.5
Pd-PVA/Al_2O_3	0.4	3.0 ± 0.8		14.5	30.5
Pd/Al_2O_3	5.0	2.1 ± 0.4		16	

[a] According to CO chemisorption in aqueous phase [15].

Also, the changes in integrated areas of fitted peaks with time during the full experiment (adsorption of nitrite, flushing with inert and reducing of adsorbed species in H_2 containing water) as shown in Fig. 4(d) have been discussed in detail previously [19]. In short, linearly and multi-bonded NO, together with NH_2 were detected as stable N-containing species chemisorbed on the Pd surface by reactive adsorption of nitrite. Multi-bonded NO was not detected in our original study [19,20], which will be discussed in detail in the near future [21]; it should be noted this is not essential for the discussion here. NH_4^+ was formed initially when nitrite was introduced to the H_2 pre-treated Pd surface, decreasing rapidly because of exhaustion of adsorbed hydrogen as well as weak interaction of NH_4^+ with the catalyst [20]. Flushing with Ar/H_2O induced removal of nitrite in solution. Subsequent exposure to H_2/H_2O induces removal of NO (L) and NO (M) first, followed by consumption of NH_2, accompanied by formation of ammonium. All this has been discussed in detail [19] and is actually not essential for this study. However, the sequence is needed to generate a catalyst that mimics the situation at the end of a batch experiment, as will be discussed later.

Fig. 4(d) shows that the NO (L) and NO (M) species, as well as free NO_2^- in aqueous phase were completely removed after flushing with H_2O saturated with H_2 for 10 min, while most of NH_2 species was also consumed and the integrated area became stable. The decrease of NH_4^+ indicates a decrease of the formation rate. After 10 min flushing with H_2/H_2O, only NH_4^+ and NH_2 were detectable by ATR-IR. After 55 min the flow was changed to recycling while feeding H_2 through the membrane, as described in the experimental section.

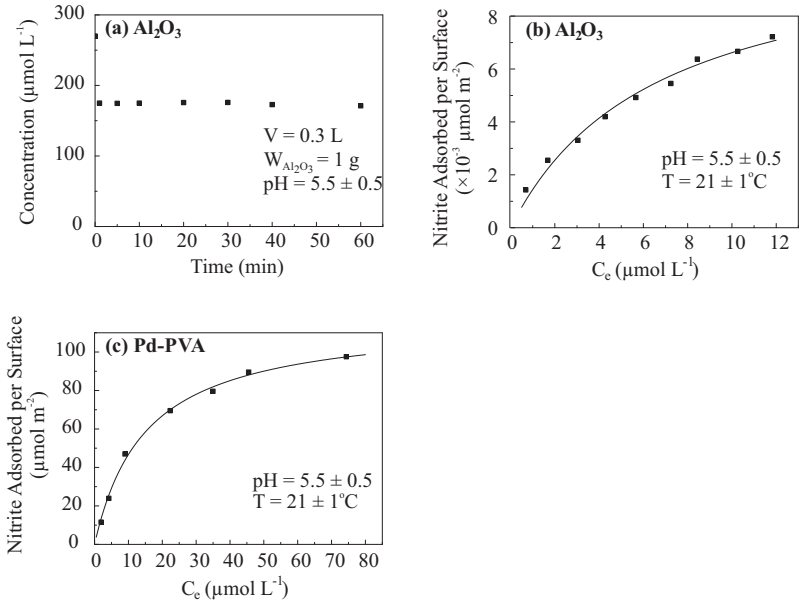

Fig. 2. Adsorption of nitrite by Al_2O_3: (a) nitrite concentration with Al_2O_3 as function of time; nitrite adsorption isotherm with (b) Al_2O_3 and (c) Pd-PVA colloid. The lines represent fitting of the data using the Langmuir isotherm. The surface area of Pd colloid was determined by CO chemisorption in aqueous phase [15], and surface area of Al_2O_3 was determined by N_2 physisorption with BET method (Table 1).

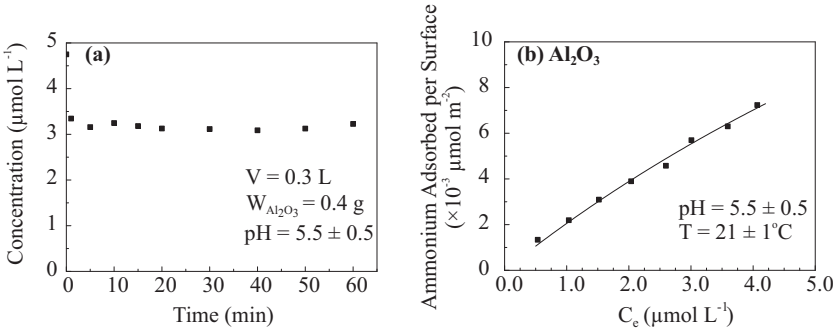

Fig. 3. Adsorption of ammonium by Al_2O_3: (a) ammonium concentration as function of time; (b) Ammonium adsorption isotherm. The line represents Langmuir fitting of the data. Surface area of Al_2O_3 was determined by N_2 physisorption with BET method (Table 1).

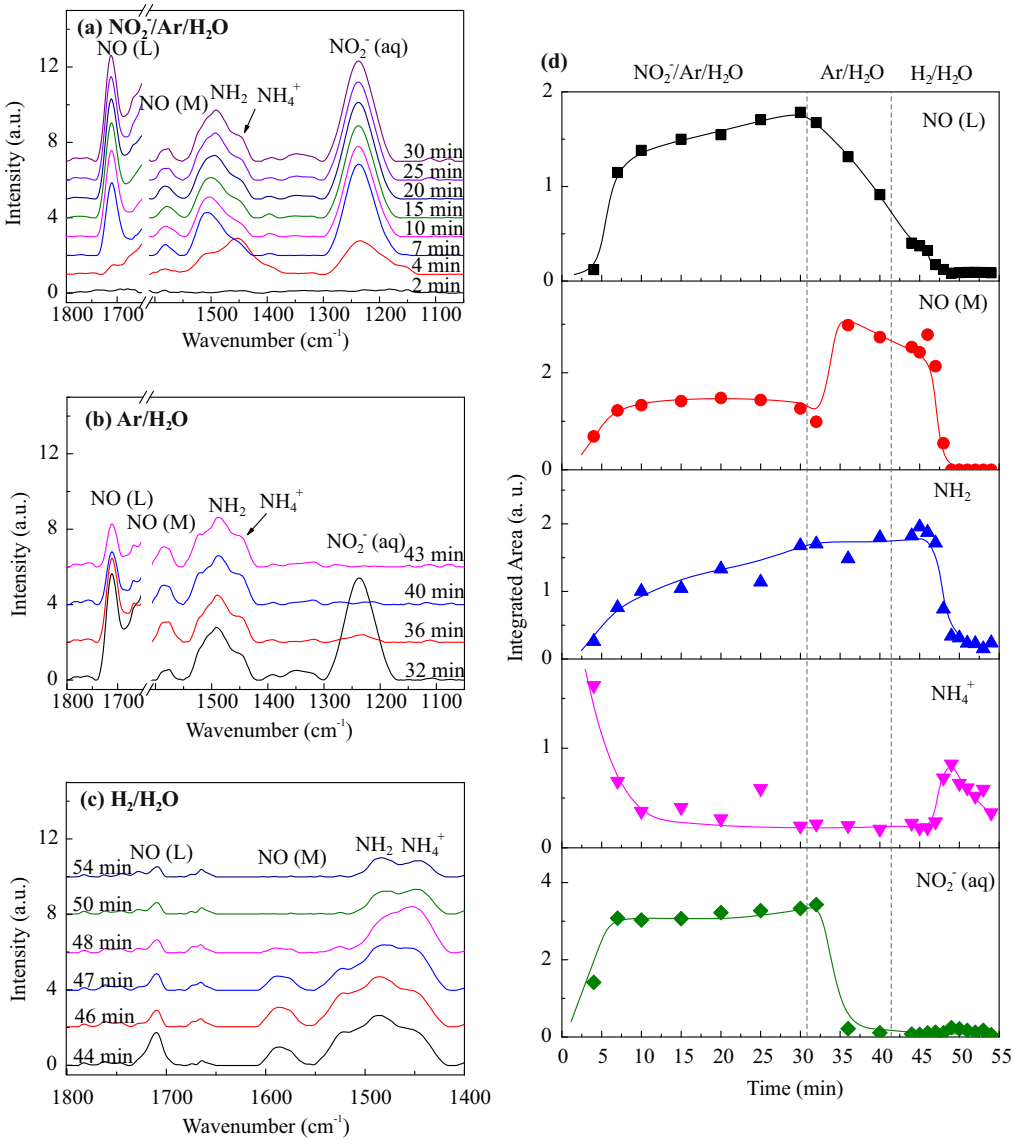

Fig. 4. ATR-IR spectra of N-containing-species on Pd/Al_2O_3 catalyst during (a) nitrite adsorption on H_2 pre-reduced Pd/Al_2O_3, followed by (b) flushing with Ar/H_2O, and then (c) titration with H_2/H_2O. (d) Summary of change of integrated peak areas during the three steps. The experiment was performed at $T = 21$ °C and pH 7.

Fig. 5 shows both the amount of adsorbed NH_2 and the amount of NH_4^+ increased during circulation while hydrogen is continuously supplied. The concentration of both species reached a maximum during recirculation for 3 h.

3.5. Nitrite hydrogenation

Fig. 6 shows the concentration of nitrite and ammonium as function of time with unsupported Pd-PVA colloid as well as

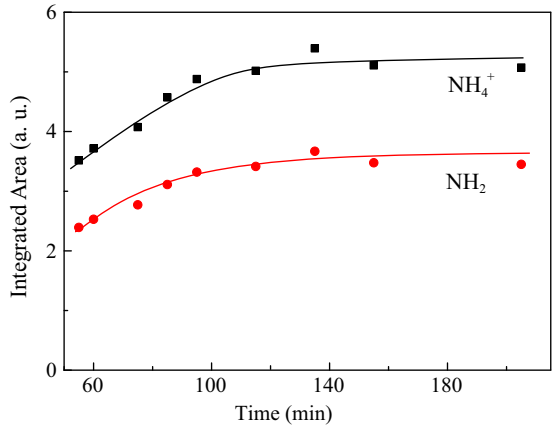

Fig. 5. Integrated area of fitted peaks of NH_2 and NH_4^+ catalyst in ATR-IR spectra with Pd/Al_2O_3 during recirculation.

Pd-PVA supported on Al_2O_3. The concentration of Pd in the experiments is summarized in Table 2. As shown in Fig. 6(a), nitrite concentration decreased from 435 μmol L^{-1} to 0.5 μmol L^{-1} within 1 h. In the same time, ammonium concentration increased to 1.4 μmol L^{-1} as can be seen in Fig. 6(c) and Table 2. The change in the slope in the inset of Fig. 6(c) also shows that the formation rate of ammonium decreased significantly, from 0.043 μmol L^{-1} - min^{-1} to 0.008 μmol L^{-1} min^{-1}, at the moment that nitrite is exhausted after about 65 min, when the concentration of nitrite decreased below the detection limit of the IC (~0.5 μmol L^{-1}). Ammonium formation continued during the following 40 h, despite the fact that nitrite is exhausted, reaching a final ammonium concentration of 7.4 μmol L^{-1}.

Similar results are obtained with Pd-PVA supported on Al_2O_3; again, final ammonium concentration was reached after at least 20 h, whereas nitrite was completely consumed much earlier, as shown in Fig. 6(b) and (d). The final ammonium concentrations increased with increasing weight of Pd-PVA/Al_2O_3 catalyst from 50 mg to 200 mg, as shown in Fig. 6(d) and Table 2.

Fig. 7 is based on the data presented in Fig. 6, showing that the selectivity to ammonium remained very low until the nitrite conversion approached 100%, suddenly inducing a significant increase in the selectivity to ammonium. The selectivity to ammonium is not influenced by the amount of Pd-PVA/Al_2O_3 catalyst, until the conversion approaches 100%, as shown in Fig. 7(b), inducing an increase in final selectivity to ammonium when increasing the amount of catalyst.

Similar experiments were performed with Pd/Al_2O_3 and the results are presented in Fig. 8 and Table 2. Fig. 8(a) shows again rapid conversion of nitrite as well as formation of ammonium after 30 min, after exhaustion of nitrite. The ammonium concentration continued to increase for another 3 h to 25 μmol L^{-1}. The selectivity to ammonium increased slowly to 1% at 99% nitrite conversion. Despite the fact this 1% selectivity to ammonia is higher as compared to Pd-PVA and Pd-PVA/Al_2O_3, also in this case a significant increase in selectivity to ammonium was observed when approaching complete conversion of nitrite beyond 99%, as shown in Fig. 8(b).

As shown in Fig. S-1, both Pd-PVA/Al_2O_3 and Pd/Al_2O_3 operated in a continuous flow fixed-bed reactor show stable activity for 3–4 h after a short stabilization period governed by hydrodynamics, agreeing with previous publication using a continuous operated reactor showing no significant deactivation even over 30 h [13]. On the other hand, the reaction rate is obvious slower in a second run of semi-batch operation with Pd-PVA colloid, as compared with the first run to achieve 95% nitrite conversion, as shown in Fig. S-2. The difference is in order of a fact of 2.

4. Discussion

4.1. Nitrite hydrogenation at low conversion level

Table 2 shows that the TOFs are quite similar for Pd-PVA/Al_2O_3 and Pd/Al_2O_3 catalysts, confirming that PVA has no influence on the intrinsic activity of Pd as discussed in our previous work [15]. However, a much lower TOF was observed for unsupported

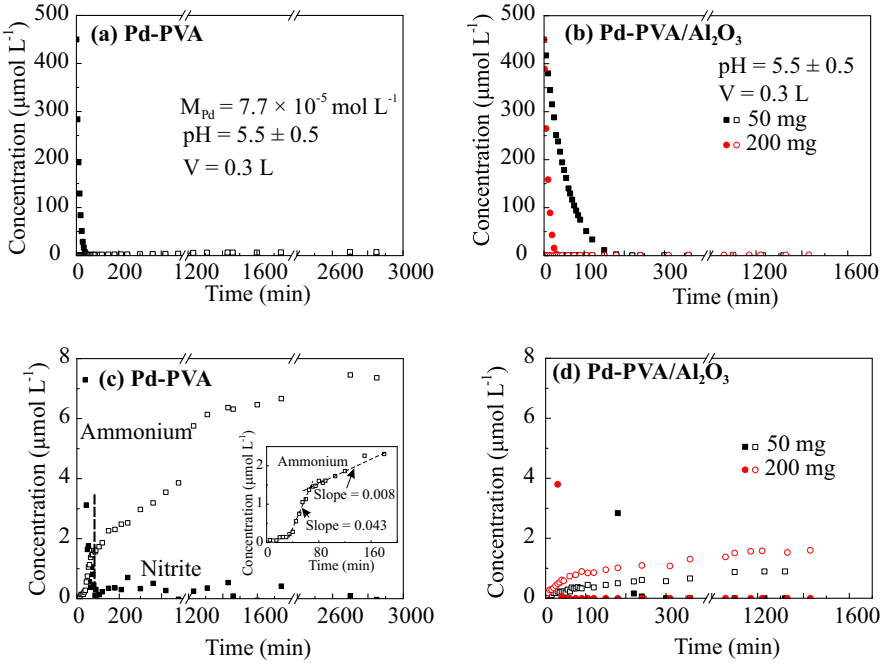

Fig. 6. Concentration of nitrite (solid symbols) and ammonium (open symbols) as function of time with (a) unsupported Pd-PVA colloid and (b) Pd-PVA supported on Al_2O_3; (c) and (d) provide a zoom-in of the data presented in (a) and (b). Note that the time axis in interrupted.

Table 2
Experimental details and results of the catalytic experiments.

Sample	W_{cat} (mg)	C_{Pd} (μmol L^{-1})	$M_{Pd,surf}$ (μmol)	TOF[a] (min^{-1})	$C_{NH_4^+,final}$ (μmol L^{-1})	$\Delta M_{NH_4^+}$ (μmol)[b]	$\Delta C_{NH_4^+}$ (μmol L^{-1})[c]	$M_{NH_4^+,ad}$ (μmol)[d]	$\frac{\Delta M_{NH_4^+}}{M_{Pd,surf}}$
Pd-PVA		77	2.1[e]	17	7.4	1.7	5.8		0.82
Pd-PVA/Al_2O_3	50	6.4	0.11	74	0.9	0.09	0.3	0.1	0.82
	200	25	0.42	95	1.6	0.30	0.9	0.4	0.71
Pd/Al_2O_3	50	79	3.9	86	28	3.6	12		0.92

[a] Based on initial reaction rate with $C_{nitrite}$ = 450 μmol L^{-1}.
[b] The increase of ammonium amount after exhaustion of nitrite (concentration < 0.5 μmol L^{-1}) in the batch reactor.
[c] The increase of ammonium concentration after exhaustion of nitrite (concentration < 0.5 μmol L^{-1}) in the batch reactor.
[d] The amount of ammonium adsorbed on Al_2O_3 at final ammonium concentration as estimated according to the adsorption isotherm in Fig. 3(b).
[e] According to CO chemisorption in aqueous phase.

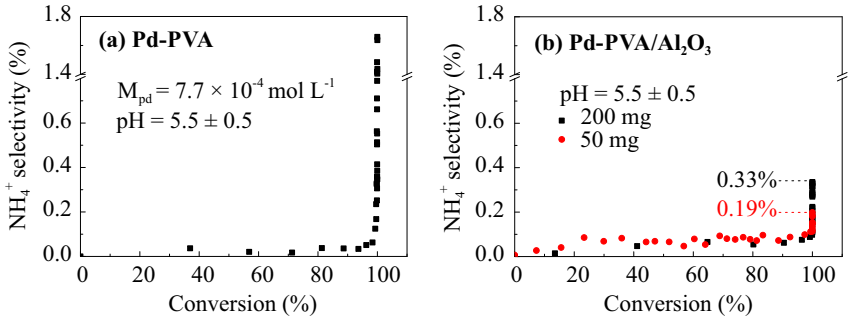

Fig. 7. Ammonium selectivity as function of nitrite conversion: (a) unsupported Pd-PVA; (b) Pd-PVA supported on Al_2O_3 for two catalyst amounts, 50 mg and 200 mg.

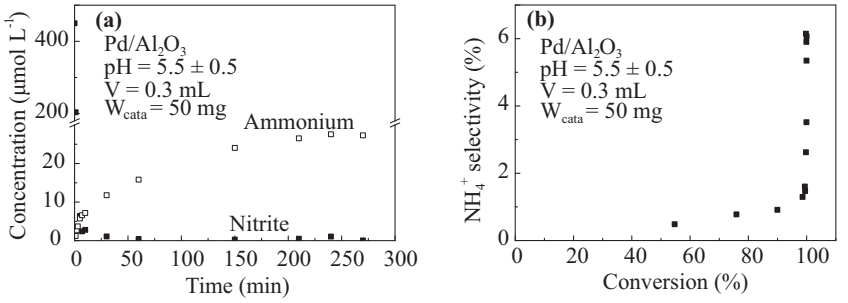

Fig. 8. Concentration of nitrite (solid symbols) and ammonium (open symbols) as function of time with Pd/Al_2O_3 without PVA capping.

Pd-PVA. Note that different CO chemisorption methods were used for unsupported and supported Pd NPs: the number of accessible Pd surface sites was determined by CO chemisorption in aqueous phase, whereas it was determined by gas phase CO chemisorption for the supported catalysts (Pd-PVA/Al_2O_3). Based on these results it was estimated that about 20% of the Pd surface was accessible for CO in case of Pd-PVA in aqueous phase, whereas 40% of the Pd surface is accessible for CO in case of Pd-PVA/Al_2O_3 in gas phase, based on comparison with TEM results [15]. Consequently, the TOF for Pd-PVA/Al_2O_3 is probably underestimated and despite that higher than that for Pd-PVA. Two possible speculative explanations can be proposed to explain the difference between the TOFs. First, significant interaction between Pd NPs and the Al_2O_3 surface, based in the TEM images in Fig. 1, influencing the shape of the Pd particles, might influence the activity. Second, accessibility of the Pd surface for nitrite may be influenced by the negative charge surrounding the Pd NPs (Table 1). This negative charge is likely to repulse nitrite ions, whereas positive charge of Pd-PVA/Al_2O_3 favors the adsorption of nitrite.

Figs. 7 and 8(b) show that the selectivity to ammonium increased mildly with nitrite conversion for unsupported Pd-PVA colloid, Pd-PVA/Al_2O_3 as well as Pd-Al_2O_3 catalysts. Similar increase of selectivity to ammonium with nitrate conversion with Pd-Cu/Al_2O_3 catalyst was reported by Pintar et al. [22,23]. Kinetic studies on nitrite hydrogenation agreed that formation of ammonium is favored over N_2 at low nitrite/hydrogen ratios [24,25]. Similar results were also reported by Chaplin et al. with Pd-In/Al_2O_3 catalyst in fixed bed reactor for nitrate hydrogenation [12]. Ebbesen et al. confirmed that decreasing nitrite/hydrogen ratio enhances the formation of intermediates responsible for the formation of ammonium, based on studies using ATR-IR [19,20]. Hence, the increase in selectivity to ammonium with nitrite conversion can be simply explained based on kinetics, for conversion levels below 99.9% ($C_{nitrite}$ > 0.5 μmol L^{-1}). Another explanation proposed in the literature, i.e. the pH decreases with conversion enhancing ammonium formation, is not relevant here because CO_2 was used to buffer [24].

4.2. Reaction after exhaustion of dissolved nitrite

Surprisingly, the selectivity to ammonium increased significantly when approaching complete conversion for all three catalysts, as shown in Figs. 7 and 8(b). Fig. 6(c) and Table 2 show that ammonium formation continued during tens of hours after nitrite exhaustion ($C_{nitrite}$ < 0.5 μmol L^{-1}) with unsupported Pd-PVA colloid. The ammonium concentration increased by

6.0 μmol L^{-1} in this time window, which clearly shows that the reactant involved cannot be dissolved nitrite. Similar deviations in the mass balance were found with Pd-PVA/Al_2O_3 and Pd/Al_2O_3 catalysts as shown in Figs. 6(d), 8, and Table 2. In all cases, the amount of ammonia formed after exhaustion of nitrite exceeds significantly the detection limit of nitrite. Apparently, the extra nitrogen must origin from adsorbed species on the catalysts, which is further confirmed by the increase of ammonium formation after nitrite exhaustion with increasing Pd-PVA/Al_2O_3 catalyst amount, as shown in Fig. 6(d) and Table 2. Two options would seem reasonable to explain this observation: nitrite may adsorb on Pd, alumina or PVA, acting as a reservoir of nitrite. Alternatively, N-containing intermediate species are likely to be adsorbed on the Pd surface, which possibly act as reservoirs. We will first consider adsorption of nitrite.

Nitrite adsorption on Al_2O_3 can be neglected as compared to the amount of nitrite adsorbed on Pd and PVA, as shown in Fig. 2. The low surface coverage of nitrite on alumina is at least an order of magnitude too small to account for the formation of ammonia after nitrite exhaustion. Furthermore, the concentration increase of ammonium formed after exhaustion of nitrite exceeds significantly the detection limit of nitrite (0.5 μmol L^{-1}) for unsupported Pd-PVA as well as Pd-PVA/Al_2O_3. Thus, adsorption of nitrite on alumina cannot be responsible for this effect. Furthermore, the same was also observed with Pd/Al_2O_3, in the absence of any PVA, as shown in Fig. 8 and Table 2, indicating that also PVA is not relevant for the ammonium increase after nitrite exhaustion. Finally, the amount of ammonium formed increased with increasing amount of Pd, as shown in Table 2. Thus, the formation of ammonium is due to either adsorbed nitrite or other N-containing species on the Pd surface. For further discussion of the effect of PVA on the catalytic properties of Pd nano-particles we refer to previous work [15].

It is well known that adsorption of nitrite on Pd in the presence of hydrogen results in the formation of adsorbed species including NO and NH_2, based on previous ATR-IR studies [19], similar to the results in Fig. 4. These nitrogen-containing species are relevant for the formation of the extra ammonium after nitrite exhaustion, as some of those species (e.g. NH_2) is converted to ammonium when flushing with H_2 containing water [19]. This is further supported by the fact that the molar ratio of the extra ammonium formed and the number of Pd surface atoms ($\Delta M_{NH_4^+}/M_{Pd,surf}$) is in the range between 0.7 and 0.9 for all the catalysts, as shown in Table 2. The data for Pd/Al_2O_3 are obviously more reliable than for the PVA containing samples, as the number of accessible Pd surface atoms is measured with CO chemisorption in a straightforward way. Instead, for the PVA containing catalysts uncertainty exists whether the effect of blocking Pd surface sites with PVA is correctly accounted for. In any case, the data show that the accessible Pd surface area is significantly covered with this N-containing species for all three types of catalyst, independent of presence or absence of PVA.

In summary, significant amount of ammonium formed when approaching complete conversion of nitrite during hydrogenation in a semi-batch reactor. This causes a deviation in the apparent nitrogen mass balance during this period. The extra nitrogen released into the aqueous phase as ammonium is caused by adsorbed N-containing species on the Pd surface.

4.3. N-containing species on Pd NPs

ATR-IR study with circulation flow with continuous hydrogen supply was performed to identify N-containing-species responsible for the formation of ammonium, after exhaustion of nitrite in the semi-batch experiment. As shown in Fig. 5, exclusively NH_2 and NH_4^+ were detected during the circulation [20]. The peak area of NH_2 and NH_4^+ increased in the same time, whereas no other nitrogen-containing species were detected on the catalyst surface. The formation of ammonium is consistent with the formation of ammonium at the end of the semi-batch experiment as discussed above. NH_2 species is proposed to be an intermediate in the pathway to NH_4^+ formation [19]. Apparently, formation of NH_2 and NH_4^+ originates from a nitrogen-containing species on Pd surface that cannot be detected with IR. We propose that nitrogen atoms on the Pd surface are responsible for the effect, as any species containing N and either O or H would be IR active.

It should be noted that the experiment in Fig. 5 was performed during only 3 h because of experimental limitations, significantly shorter than the time needed to obtain the final amount of ammonium in a batch experiment (Fig. 3). It is expected that after longer times the surface coverage of NH_2 would decrease under formation of additional ammonium.

As discussed above, Table 2 shows $\Delta M_{NH_4^+}/M_{Pd,surf}$ ratios in the range of 0.7–0.9 for all catalysts, indicating that the surface coverage of nitrogen atoms is significant. Fig. 6(c) shows that the formation rate of ammonium significantly decreased after exhaustion of nitrite, indicating that the reaction rate of adsorbed N atoms to ammonium is significantly slower than the rate of ammonium formation during the reaction in the presence of nitrite in solution. It can be concluded that, when approaching complete conversion, the Pd surface is significantly covered with almost unreactive N-atoms. The reaction pathway to ammonium during nitrite hydrogenation is faster and apparently does not involve these nitrogen atoms. Furthermore, N_2 formation by coupling of two N-atoms is apparently even slower, because otherwise no ammonium would form after nitrite is completely converted. Clearly, formation of N_2 is orders of magnitude faster in the presence of nitrite, which can be explained by assuming that formation of N_2 proceeds via N_2O that likely forms via adsorbed N with adsorbed NO. Direct conversion of NO to N_2O has been suggested as dominant pathway for the formation of N_2 in both chemical and electrochemical reductions of nitrite [11,19,26]. N-atoms cover a large fraction of the Pd surface when approaching complete nitrite conversion, acting as pseudo-spectator species, as these N-atoms are insufficient reactive to contribute to the formation on N_2, although they can be very slowly converted to ammonium. It should be noted that the very low reactivity of these N-atoms is not caused by catalyst deactivation, as deactivation of the catalyst (see SI), if any, is insignificant as compared to the fact that hydrogenation of N-atoms is orders of magnitude slower than the rate of nitrite hydrogenation.

In general, this example shows that a detailed study of the event after complete conversion of the reactant may reveal details of the mechanism of the reaction. This opportunity has not been utilized in general at this point.

From a practical point of view, the effect reported here should be avoided to limit the formation of ammonium. This can be achieved by stopping the reaction of nitrate/nitrite hydrogenation before reaching complete conversion, in order to limit the formation of ammonium in case of batch operation. Alternatively, fixed bed operation would also avoid this problem and therefore would be recommended for purification of drinking water.

5. Conclusions

Nitrite hydrogenation was studied with Pd catalysts prepared with colloid method and impregnation. The selectivity to ammonium increased significantly when approaching complete conversion of nitrite, which is caused by formation of ammonium when nitrite is completely converted. It is concluded that nitrogen atoms, covering about 80% of the accessible Pd surface area, convert very

slowly to ammonium. These N atoms are almost unreactive, and neither the formation of ammonium via hydrogenation, nor the formation of N_2 via dimerization contribute significantly during steady-state operation.

Acknowledgments

The authors gratefully acknowledge financial support from China Scholarship Council. We are highly grateful to the constructive suggestions of Prof. Yongdan Li from Tianjin University, China. The authors are also grateful to R. Brunet Espinosa for fixed-bed testing, M. Smithers for TEM, J.A.M. Vrielink and T.L.M. Velthuizen for BET and XRF measurements, and K. Altena-Schildkamp for CO-chemisorption measurements. We acknowledge B. Geerdink for technical support.

Appendix A. Supplementary material

Supplementary data associated with this article can be found, in the online version, at http://dx.doi.org/10.1016/j.jcat.2016.02.007.

References

[1] K.-D. Vorlop, T. Tacke, Chemie Ingenieur Technik 61 (1989) 836–837.
[2] T. Tacke, Dissertation, Technischen Universität Carolo-Wilhelmina, 1991.
[3] S. Hörold, K.D. Vorlop, T. Tacke, M. Sell, Catal. Today 17 (1993) 21–30.
[4] J.C. Fanning, Coord. Chem. Rev. 199 (2000) 159–179.
[5] M. Shrimali, K.P. Singh, Environ. Pollut. 112 (2001) 351–359.
[6] A. Kapoor, T. Viraraghavan, J. Environ. Eng. 123 (1997) 371–380.
[7] N. Barrabés, J. Sá, Appl. Catal., B 104 (2011) 1–5.
[8] F. Gauthard, F. Epron, J. Barbier, J. Catal. 220 (2003) 182–191.
[9] N. Wehbe, M. Jaafar, C. Guillard, J.-M. Herrmann, S. Miachon, E. Puzenat, N. Guilhaume, Appl. Catal., A 368 (2009) 1–8.
[10] A.E. Palomares, C. Franch, A. Corma, Catal. Today 149 (2010) 348–351.
[11] K.A. Guy, H. Xu, J.C. Yang, C.J. Werth, J.R. Shapley, J. Phys. Chem. C 113 (2009) 8177–8185.
[12] B. Chaplin, J. Shapley, C. Werth, Catal. Lett. 130 (2009) 56–62.
[13] J.K. Chinthaginjala, J.H. Bitter, L. Lefferts, Appl. Catal., A 383 (2010) 24–32.
[14] D. Shuai, J.K. Choe, J.R. Shapley, C.J. Werth, Environ. Sci. Technol. 46 (2012) 2847–2855.
[15] Y. Zhao, J.A. Baeza, N. Koteswara Rao, L. Calvo, M.A. Gilarranz, Y.D. Li, L. Lefferts, J. Catal. 318 (2014) 162–169.
[16] Y. Yoshinaga, T. Akita, I. Mikami, T. Okuhara, J. Catal. 207 (2002) 37–45.
[17] Y. Zhao, L. Jia, J.A. Medrano, J.R.H. Ross, L. Lefferts, ACS Catal. 3 (2013) 2341–2352.
[18] S.D. Ebbesen, B.L. Mojet, L. Lefferts, Langmuir 22 (2005) 1079–1085.
[19] S.D. Ebbesen, B.L. Mojet, L. Lefferts, J. Catal. 256 (2008) 15–23.
[20] S.D. Ebbesen, B.L. Mojet, L. Lefferts, Langmuir 24 (2008) 869–879.
[21] N. Koteswara Rao, A. van Houselt, B.L. Mojet, L. Lefferts, in preparation.
[22] A. Pintar, M. vetinc, J. Levec, J. Catal. 174 (1998) 72–87.
[23] A. Pintar, J. Batista, J. Hazard. Mater. 149 (2007) 387–398.
[24] A. Pintar, G. Berčič, J. Levec, Aiche J. 44 (1998) 2280–2292.
[25] J.K. Chinthaginjala, L. Lefferts, Appl. Catal., B 101 (2010) 144–149.
[26] M. Duca, B. van der Klugt, M.T.M. Koper, Electrochim. Acta 68 (2012) 32–43.